JCI insight

RESEARCH ARTICLE

A unique mutator phenotype reveals complementary oncogenic lesions leading to acute leukemia

Mianmian Yin,[1] Timour Baslan,[2] Robert L. Walker,[1] Yuelin J. Zhu,[1] Amy Freeland,[3] Toshihiro Matsukawa,[1] Sriram Sridharan,[4] André Nussenzweig,[4] Steven C. Pruitt,[3] Scott W. Lowe,[2,5] Paul S. Meltzer,[1] and Peter D. Aplan[1]

[1]Genetics Branch, Center for Cancer Research, National Cancer Institute, NIH, Bethesda, Maryland, USA. [2]Cancer Biology and Genetics Program, Sloan Kettering Institute, Memorial Sloan Kettering Cancer Center, New York, New York, USA. [3]Department of Molecular and Cellular Biology, Roswell Park Cancer Institute, Buffalo, New York, USA. [4]Laboratory of Genome Integrity, National Cancer Institute, NIH, Bethesda, Maryland, USA. [5]Howard Hughes Medical Institute, Chevy Chase, Maryland, USA.

Mice homozygous for a hypomorphic allele of DNA replication factor minichromosome maintenance protein 2 (designated *Mcm2*$^{cre/cre}$) develop precursor T cell lymphoblastic leukemia/lymphoma (pre-T LBL) with 4–32 small interstitial deletions per tumor. Mice that express a *NUP98-HOXD13* (*NHD13*) transgene develop multiple types of leukemia, including myeloid and T and B lymphocyte. All *Mcm2*$^{cre/cre}$ *NHD13*$^{+}$ mice develop pre-T LBL, and 26% develop an unrelated, concurrent B cell precursor acute lymphoblastic leukemia (BCP-ALL). Copy number alteration (CNA) analysis demonstrated that pre-T LBLs were characterized by homozygous deletions of *Pten* and *Tcf3* and partial deletions of *Notch1* leading to *Notch1* activation. In contrast, BCP-ALLs were characterized by recurrent deletions involving *Pax5* and *Ptpn1* and copy number gain of *Abl1* and *Nup214* resulting in a *Nup214-Abl1* fusion. We present a model in which Mcm2 deficiency leads to replicative stress, DNA double strand breaks (DSBs), and resultant CNAs due to errors in DNA DSB repair. CNAs that involve critical oncogenic pathways are then selected in vivo as malignant lymphoblasts because of a fitness advantage. Some CNAs, such as those involving *Abl1* and *Notch1*, represent attractive targets for therapy.

Introduction

DNA replicative stress, typically in response to oncogene-induced hyperproliferation, has been linked to malignant transformation (1–3). Although the precise mechanisms by which replicative stress might result in cancer remain unknown, it is thought that chronic replicative stress leads to replication fork stalling, collapse, and subsequent DNA double strand breaks (DSBs) at or near the site of replication fork collapse (2). Inefficient repair of these DNA DSBs leads to genomic instability reflected by indels and structural variations involving genes important for malignant transformation (2).

Minichromosome maintenance complex component 2 (*Mcm2*) is a core component of the DNA replication-licensing complex required for replication initiation during S phase. A multi-subunit complex containing Mcm2–7 is responsible for the initial unwinding of DNA (4, 5). We previously generated a mouse strain containing a CreERT2 cassette flanked by an IRES knocked into the 3′ UTR of *Mcm2*, creating an Mcm2$^{\text{IRES–CreERT2}}$ allele (henceforth referred to as *Mcm2*^{cre}) (6). Unexpectedly, this knockin allele resulted in diminished expression of Mcm2 protein. *Mcm2*$^{cre/cre}$ mouse embryo fibroblasts expressed approximately one-third the amount of Mcm2 protein compared with wild-type (WT) controls. Remarkably, almost all *Mcm2*$^{cre/cre}$ mice develop a lethal precursor T cell lymphoblastic leukemia/lymphoma (pre-T LBL) within 4 months of age. Previous studies identified abnormal karyotypes and increased levels of chromosome breaks in cultured cells with reduced expression of Mcm proteins (7, 8), and array comparative genomic hybridization demonstrated that pre-T LBL in *Mcm2*$^{cre/cre}$ mice had numerous small (average < 0.5 Mbp) genomic deletions, including several genes known to be relevant for human pre-T LBL, such as *E2a* (*Tcf3*) and *Pten* (9), leading to the hypothesis that *Mcm2* deficiency led to deletions of important tumor suppressor

Conflict of interest: PDA receives royalties from the NIH Technology Transfer Office for the invention of NHD13 mice.

Submitted: June 28, 2019
Accepted: October 10, 2019
Published: December 5, 2019.

Reference information: *JCI Insight*. 2019;4(23):e131434. https://doi.org/10.1172/jci.insight.131434.

genes, resulting in malignant transformation. These findings led us to view *Mcm2*$^{cre/cre}$ cells as a potential tool for inducing mutation, analogous to ionizing radiation (10), ethylnitrosourea (11), or retroviral insertion (12). In this view, dysregulation of Mcm2 protein is not directly oncogenic; instead, Mcm2 dysregulation leads to widespread genomic deletions, some of which are oncogenic. Cells that undergo a combination of mutations that dysregulate several complementary, collaborative pathways are selected in vivo because of a fitness advantage and emerge as a malignancy.

A *NUP98-HOXD13* (*NHD13*) fusion gene has been identified in patients with myelodysplastic syndrome (MDS) and acute myeloid leukemia (AML) (13). Expression of an *NHD13* fusion in the hematopoietic compartment of mice led to overexpression of *Hoxa* cluster genes and resulted in a highly penetrant MDS phenotype (14). Approximately 80% of *NHD13* mice develop acute leukemia, most commonly AML, with the remainder dying from complications of MDS, such as severe anemia or infection, without signs of leukemic transformation (14). Leukemic transformation was frequently associated with spontaneous mutations of *Nras*, *Kras*, or *Cbl*, suggesting that these mutations collaborated with the *NHD13* fusion and were biologically selected in vivo (15).

In addition to targeted resequencing of candidate genes, retroviral insertional mutagenesis (RIM) identified genes whose overexpression would collaborate with an *NHD13* transgene to induce AML (16). Although RIM can identify gene inactivation events as well as gene activation events, tumor suppressor genes have typically not been identified through RIM screens, perhaps because 2 alleles need to be targeted for complete inactivation of many tumor suppressor genes, as opposed to a single allele for gene activation events (17). We hypothesized that the unique "deleter" phenotype found in *Mcm2*$^{cre/cre}$ mice could be used to identify tumor suppressor genes in the context of AML, by crossing the *NHD13* transgene onto an *Mcm2*$^{cre/cre}$ background.

Results

Mcm2$^{cre/cre}$ *NHD13*$^{+}$ *mice do not develop AML*. To determine whether *Mcm2*-deficient mice (*Mcm2*$^{cre/cre}$) can be used to identify tumor suppressor genes important for the development of AML, we generated *Mcm2*$^{cre/cre}$ *NHD13*$^{+}$ mice. Similar to prior studies, Mcm2 protein expression in thymus from 1-month-old *Mcm2*$^{cre/cre}$ mice was only 28% that of WT mice; addition of the *NHD13* transgene had no effect on the Mcm2 protein level (Supplemental Figure 1; supplemental material available online with this article; https://doi.org/10.1172/jci.insight.131434DS1). Mice were euthanized when they presented with signs of leukemia, including weight loss, kyphosis, lethargy, visible lymphadenopathy, and dyspnea. *Mcm2*$^{cre/cre}$ mice had a markedly decreased survival compared with mice that were heterozygous for this allele (Figure 1A), and adding the *NHD13* transgene to the *Mcm2*$^{cre/cre}$ mice (*Mcm2*$^{cre/cre}$ *NHD13*$^{+}$) led to a modest but significant decrease in survival. Previous reports had demonstrated that *Mcm2*$^{cre/wt}$ mice were not predisposed to malignancy (6). To determine whether they had a subtle predisposition toward myeloid malignancy that could be uncovered by the *NHD13* transgene, we compared the median survival of *Mcm2*$^{cre/wt}$ *NHD13*$^{+}$ to *Mcm2*$^{wt/wt}$ *NHD13*$^{+}$; the median survival was not significantly different (259 vs. 324 days) (Figure 1A) and was similar to our previous reports with *NHD13*$^{+}$ mice (14, 18). In summary, these results showed that the *NHD13* transgene did not accelerate the onset of disease in heterozygous *Mcm2*$^{cre/wt}$ mice and caused a modest disease acceleration in *Mcm2*$^{cre/cre}$ mice.

Necropsy of both *Mcm2*$^{cre/cre}$ *NHD13*$^{+}$ and *Mcm2*$^{cre/cre}$ *NHD13*$^{-}$ mice revealed markedly enlarged thymus, splenomegaly, and hepatomegaly. Complete blood counts (CBCs) from the *Mcm2*$^{cre/cre}$ *NHD13*$^{-}$ cohort typically showed leukocytosis but were otherwise normal, whereas CBCs from the *Mcm2*$^{cre/cre}$ *NHD13*$^{+}$ cohort showed both leukocytosis and leukopenia, anemia, and thrombocytopenia, consistent with prior studies on *NHD13* mice (ref. 14 and Supplemental Table 1). Leukemic subtype determined by flow cytometry demonstrated all but 1 of the *Mcm2*$^{cre/cre}$ mice (with or without the *NHD13* transgene) had infiltration of thymus, bone marrow, and spleen with malignant thymocytes that stained for CD4, CD8, or both. The diagnosis of pre-T LBL was further supported by clonal VDJ or DJ rearrangements of the *Tcrb* gene (Supplemental Table 2) and infiltration of parenchymal organs, such as the liver, kidney, and lung, with CD3^{+} lymphoblasts (Supplemental Figure 2).

The stage of thymocyte differentiation was influenced by the presence of the *NHD13* transgene. Whereas most *Mcm2*$^{cre/cre}$ *NHD13*$^{+}$ mice displayed a CD4^{+}CD8^{+} (DP) immunophenotype, a wide spectrum of pre-T LBL immunophenotypes were identified in the thymus of *Mcm2*$^{cre/cre}$ *NHD13*$^{-}$ mice, including DP, CD4^{+}CD8^{het}, CD8^{+}CD4^{het}, CD4^{+}CD8^{-}, and CD4^{-}CD8^{-} (Figure 1, B and C). Notably, none of the 46 *Mcm2*$^{cre/cre}$ *NHD13*$^{+}$ mice developed an AML. The *Mcm2*$^{cre/wt}$ *NHD13*$^{+}$ and *Mcm2*$^{wt/wt}$ *NHD13*$^{+}$ mice developed disease with a similar immunophenotype, primarily AML, and less commonly pre-T LBL or B cell precursor acute lymphoblastic leukemia (BCP-ALL) (Supplemental Table 1). In summary, these results

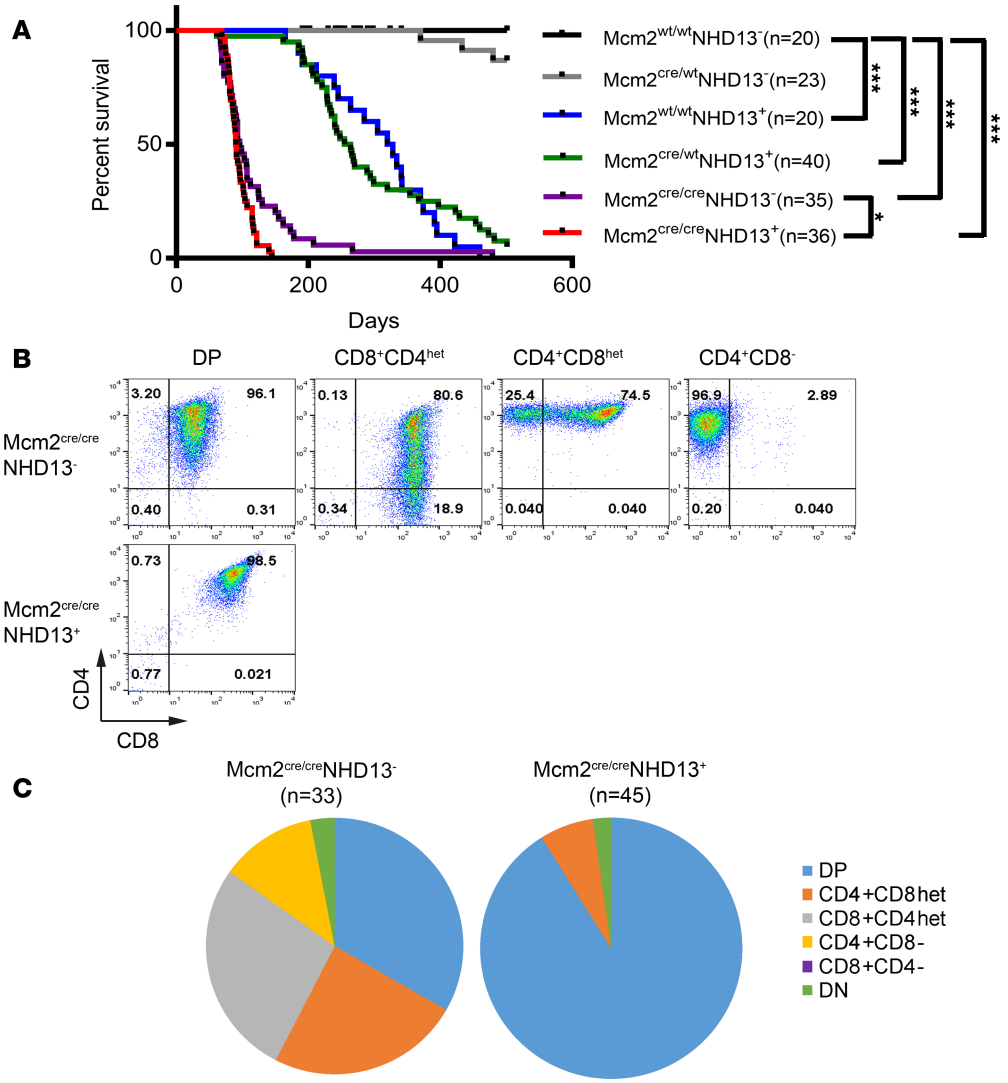

Figure 1. *Mcm2*$^{cre/cre}$ *NHD13*$^{+}$ mice do not develop AML. (**A**) Survival curve for all 6 genotypes, compared by log-rank test. *$P < 0.05$; ***$P < 0.001$. (**B**) Representative flow cytometry profile of malignant thymocytes from *Mcm2*$^{cre/cre}$ *NHD13*$^{-}$ and *Mcm2*$^{cre/cre}$ *NHD13*$^{+}$ mice with pre-T LBL. (**C**) Immunophenotype summary of pre-T LBL samples from thymus of *Mcm2*$^{cre/cre}$ *NHD13*$^{-}$ ($n = 33$) and *Mcm2*$^{cre/cre}$ *NHD13*$^{+}$ ($n = 45$) mice. DN, double negative.

demonstrated that *Mcm2*$^{cre/cre}$ *NHD13*$^{+}$ mice did not develop AML, nor did *Mcm2*$^{cre/wt}$ *NHD13*$^{+}$ mice show accelerated myeloid leukemic transformation compared with *Mcm2*$^{wt/wt}$ *NHD13*$^{+}$ transgenic mice, suggesting that this strategy did not uncover AML tumor suppressor genes.

Recurrent deletions in pre-T LBL. Based on prior studies (9), we suspected that the pre-T LBLs identified in *Mcm2*$^{cre/cre}$ *NHD13*$^{+}$ mice were initiated, at least in part, by about 0.5 Mb genomic deletions. In addition, although there was no acceleration of AML in *Mcm2*$^{cre/wt}$ *NHD13*$^{+}$ mice compared to *Mcm2*$^{wt/wt}$ *NHD13*$^{+}$ mice, we wished to determine whether *Mcm2*$^{cre/wt}$ *NHD13*$^{+}$ mice had recurrent genomic deletions. Copy number alteration (CNA) analysis for pre-T LBL and AML samples was determined by sparse whole-genome sequencing (WGS; see Methods), an approach that can accurately identify copy number losses (deletions) and gains at a resolution of roughly 125 kb and map alteration breakpoints to a resolution of approximately 25 kb (19). As anticipated, we detected 4–32 small (100–1000 kb) deletions and gains in pre-T LBL from *Mcm2*$^{cre/cre}$ samples (Figure 2A and Supplemental Figure 3, A–C), with focal deletions more common than gains (Supplemental Figure 3D).

Inspection of Figure 2A shows recurrent interstitial deletions of chromosomes 5, 6, 7, 9, 10, 12, 14, 17, and 19; *Mcm2*$^{cre/cre}$ *NHD13*$^{+}$ pre-T LBL showed a deletion pattern similar to *Mcm2*$^{cre/cre}$ *NHD13*$^{-}$ pre-T LBL. We saw no recurrent acquired copy number alterations (CNAs) in the *Mcm2*$^{cre/wt}$ *NHD13*$^{+}$ AML samples, indicating that the heterozygous *Mcm2*^{cre} allele did not predispose to recurrent deletions, even

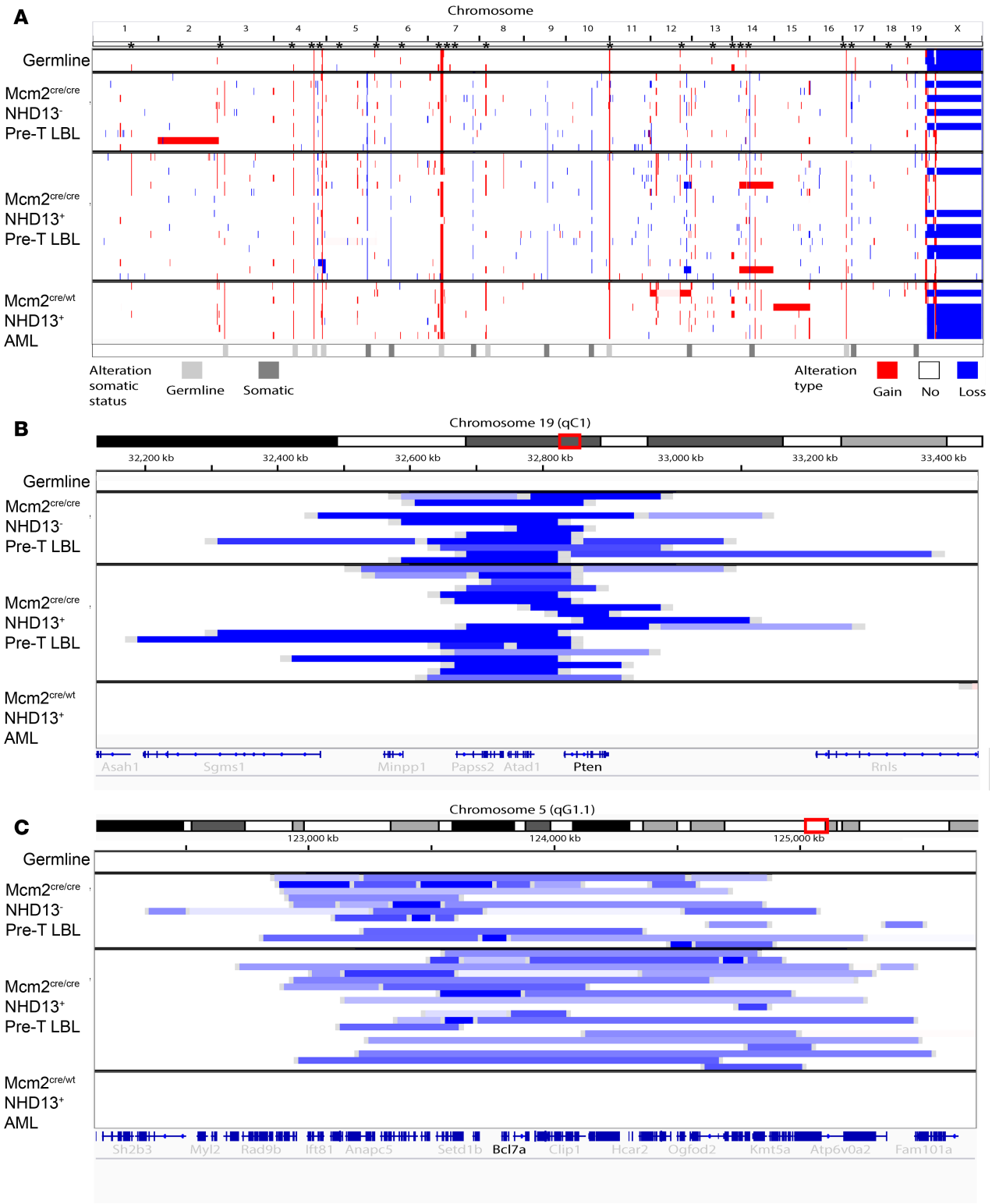

Figure 2. *Mcm2*$^{cre/cre}$ mice show recurrent deletions. (**A**) Whole-genome view of copy number alteration (CNA) analysis for germline, pre-T LBL (*Mcm2*$^{cre/cre}$ *NHD13*$^{-}$, *n* = 11 mice; and *Mcm2*$^{cre/cre}$ *NHD13*$^{+}$, *n* = 18 mice), and AML (*Mcm2*$^{cre/wt}$ *NHD13*$^{+}$, *n* = 8); samples were more than 70% tumor tissue (thymus or BM) based on flow cytometry. Mouse chromosomes 1–19 and X are indicated. (**B** and **C**) Zoomed-in view of (**B**) *Pten* (chromosome 19) and (**C**) *Bcl7a* (chromosome 5) regions. Red indicates gain; blue indicates loss. Copy number loss is proportional to color. Darker blue is consistent with homozygous loss; lighter blue suggests heterozygous loss. Asterisk indicates the gains or deletions present in germline samples compared with reference C57BL/6 genome (mm9).

in the presence of an *NHD13*-sensitizing transgene. A higher magnification view (Figure 2, B and C) demonstrates that (a) deletions can be more (e.g., *Pten*) or less (e.g., *Bcl7a*) tightly clustered, (b) deletions can be homozygous or heterozygous, and (c) no deletions are identical between different samples.

There were 15 common deleted regions (defined as deleted or gained in at least 15% of samples) in the 29 pre-T LBL primary tumors (11 $Mcm2^{cre/cre}$ $NHD13^{-}$ and 18 $Mcm2^{cre/cre}$ $NHD13^{+}$) (Supplemental Table 3); 9 regions were deleted in more than 60% of the samples. These included expected regions, such as *Tcra* and *Tcrb*, as well as previously reported regions that encompass known tumor suppressor genes, such as *Pten* (20), *Tcf3* (21), *Cdkn1a* (22), *Bcl11b* (ref. 23 Supplemental Figure 4), and *Zfp36l2* (24), and genes involved in normal T cell differentiation, including *Tcf12*, *Bcl7a*, and *Bcl7c*. A single region from chromosome 8 was recurrently amplified, specifically in $Mcm2^{cre/cre}$ $NHD13^{+}$ mice; there was no obvious candidate oncogene in this region.

To validate the small (125–1000 kb) deletions detected by sparse WGS, we performed conventional WGS, with about 28× coverage, for 3 $Mcm2^{cre/cre}$ $NHD13^{-}$ pre-T LBLs, using nonmalignant tail DNA as a germline control. WGS identified 93 genomic deletions in 3 $Mcm2^{cre/cre}$ $NHD13^{-}$ pre-T LBL (Supplemental Table 4). Eighty-five percent (57/67) of the CNAs identified by sparse WGS were verified (Supplemental Figure 5A). An additional 36 deletions were identified by WGS; most of these were smaller than 125 kb (Supplemental Table 4), consistent with the anticipated resolution of the sparse WGS method. When only deletions greater than 125 kb were considered, samples 2739 and 2854 were 100% concordant, whereas sample 2883 was only 68% concordant. One potential reason for the poor correlation in sample 2883 is the observation that this sample had substantial contamination with WT DP thymocytes (flow cytometry showed 60.5 % $CD4^{+}CD8^{het}$ and 35.9% WT $CD4^{+}CD8^{+}$ thymocytes) (Supplemental Figure 5, B–D).

Fifteen of the deleted regions involved TCR α, β, γ, or δ. Because these regions undergo programmed deletions in the course of normal development because of VDJ recombination, we focused our analysis on the remaining 78 deletions that were linked to the *Mcm2* deficiency. We identified 11 homozygous deletions in the 3 samples; these homozygous deletions included *Pten*, *Dnmt3a*, *Tcf3*, and *Bcl7a* (Supplemental Table 5). An additional 9 deletions were identified that involved adjacent, but not overlapping, regions (Supplemental Table 5). Sample 2754 had 1 large *Ikzf1* deletion, encompassing the entire gene, and a focal 9177-bp deletion, which deleted exons 4 and 5. Reverse transcriptase PCR (RT-PCR) revealed several splice forms of *Ikzf1* not seen in WT BM (Supplemental Figure 5, E–G), all missing exons 4 and 5. The interstitial deletion of *Ikzf1* and aberrant splice forms was reminiscent of *IKZF1* deletions and aberrant isoforms associated with human lymphoid leukemia (25). Detailed analysis of the sequence at the deletion junction of the 78 deleted regions in pre-T LBL samples revealed that 51 of the 78 junctions had 1–5 bp of microhomology (Supplemental Table 4). Twenty-five junctions contained nontemplated insertions at the breakpoint junctions; some of these were quite extensive, 1–50 nucleotides in length.

We next used whole-exome sequencing (WES) to determine whether small indels or single nucleotide variants (SNVs) contributed to the development of pre-T LBL. WES results revealed 104 Tier 1 mutations in the 29 pre-T LBLs, or an average of 3 per tumor. Only 6 of the 29 samples had mutations in genes known or suspected to be involved in pre-T LBL, 3 *Notch1*, 2 *Tp53*, and 1 *Ezh2* mutation (refs. 24, 26 and Supplemental Table 6). All of these mutations were confirmed (Supplemental Figure 6) by Sanger sequencing of tumor and normal tissue.

Ongoing deletions in $Mcm2^{cre/cre}$ cell lines. We established immortal, cytokine-independent cell lines from 10 $Mcm2^{cre/cre}$ pre-T LBL samples. Because the cell lines were uncontaminated by any normal tissue, we used genomic DNA from the cell lines to validate loss of DNA and protein expression (Supplemental Figure 7, A–C). The anticipated homozygous losses for *Zfp36L2*, *Tcf3*, and *Pten* were confirmed (Supplemental Figure 7A), as well as loss of Pten protein (Supplemental Figure 7C). However, sample 2773 remained positive in the PCR assay but did not produce Pten protein. A diagram of the deletions (Supplemental Figure 7B) demonstrates that although the deletions from 2773 were not overlapping, each allele had deleted substantial portions of the *Pten* coding sequence. Mcm2 protein expression was similar in the *Mcm2*-deficient cell lines and primary samples (Supplemental Figure 7D). To determine (a) whether the cell line that emerged in tissue culture represented the predominant clone in vivo and (b) whether the cell lines continued to undergo genomic deletions, we compared CNAs in primary tumor, early-passage (TCE, 1–1.5 months in culture) and late-passage (TCL, 2–6 months in culture) pre-T LBL cell lines. In all cases, the global pattern of deletions was similar to the primary tumor, indicating that the cell line that emerged in tissue culture was representative of the primary tumor (Figure 3). Deleted regions were scored for each trio and summarized in Table 1. A total of 135 deletions were identified; 90 were stable and present in all 3 samples, suggesting that these were truncal lesions. Twenty-two deletions were acquired at the

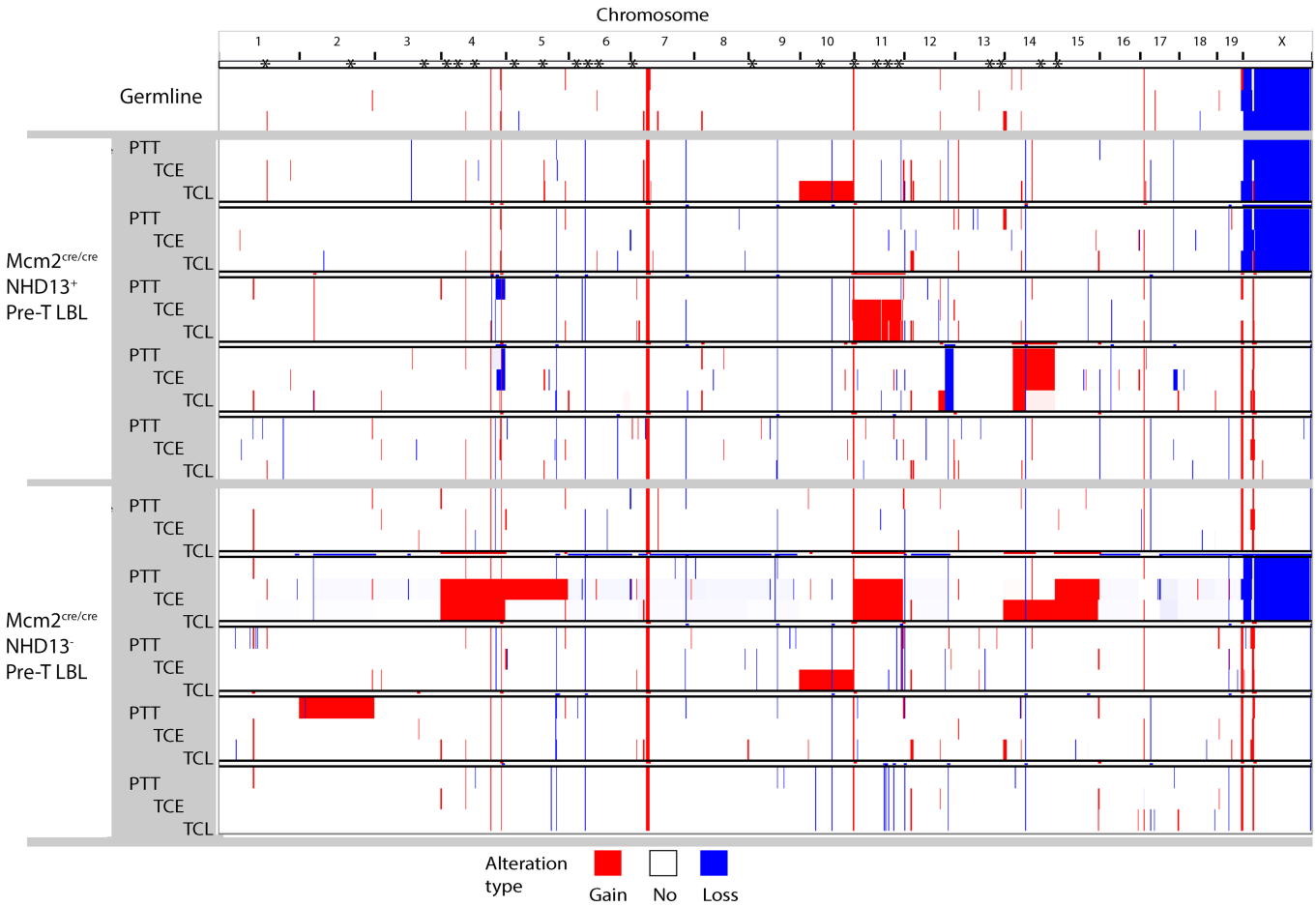

Figure 3. Stable and ongoing CNAs in *Mcm2*$^{cre/cre}$ pre-T LBL. CNAs of trios from mice 2875, 2854, 2880, 2730, 2773, 2696, 2795, 2869, 2883, and 2641 primary pre-T LBL tumor (PTT), and pre-T LBL cell line at early passage (1–1.5 months; TCE) and late passage (2–6 months; TCL). Color code as in Figure 2A.

early-passage stage; these could have been acquired during tissue culture or could have been present as a minor clone in the primary tumor. Only 10 new deletions were acquired at the late-passage stage, compared with 90 that were present initially and persistent.

To gain further insight into the frequency of ongoing deletions in the *Mcm2*$^{cre/cre}$ cell lines, we obtained single-cell clones by plating late-passage 2696 cell line at a limiting dilution. Five of 96 wells expanded and were analyzed for CNAs. Supplemental Figure 7E shows new deletions present in the single-cell clones, an average of 5 new deletions per clone compared with the late-passage cell line. These deletions involved *Rpl5*, *Cntnap2*, and *Ccdc* genes, which were not recurrently deleted in other *Mcm2*$^{cre/cre}$ pre-T LBL samples; taken together, these findings suggest that although the deleter phenotype had become less pronounced during in vitro culture, ongoing interstitial deletions could be identified in the *Mcm2*$^{cre/cre}$ cell lines.

Large Clone Capture sequencing identifies frequent Notch1 interstitial deletions. Mutations involving the extracellular heterodimerization (HD) domain and/or the C-terminal proline, glutamic acid, serine, and threonine (PEST) domain of *NOTCH1* are found in more than 50% of both human and murine pre-T LBLs (26, 27). In addition, a recurrent deletion of *Notch1* exon 1 and the adjacent 5′ regulatory sequences has been identified in mice but not humans (28, 29). This deletion leads to use of alternate *Notch1* transcript initiation upstream of exon 27 and translation initiation at M1727 within exon 28, resulting in production of a truncated Notch1 protein that lacks the extracellular ligand-binding domain, retains the transmembrane domain and sensitivity to γ-secretase inhibitors, and is functionally similar to a *NOTCH1* HD mutation (28). Given these findings, we were puzzled that only 3 *Notch1* mutations were identified by WES. Because the WGS revealed an interstitial deletion in 1 of 3 samples, we hypothesized that smaller (5–125 kb) interstitial deletions not identified in the sparse sequence CNA assay might be common events in these pre-T LBLs. "Large Clone Capture" sequencing (LCC-Seq) is a technique that allows for the custom capture and

Table 1. Summary of deletion patterns in *Mcm2*$^{cre/cre}$ pre-T LBL cell lines

PTT	+	–	–	–	+	+	+
TCE	+	+	–	+	–	+	–
TCL	+	+	+	–	+	–	–
Total with indicated pattern	90	22	10	5	1	3	4

+, deletion present; –, deletion not present.

next-generation sequencing of specific genomic regions of interest, similar in concept to WES (30). To search for *Notch1* deletions, as well as identify precise breakpoints involved in deletions, we obtained bacterial artificial chromosome (BAC) clones that covered regions of chromosomes 2 (*Notch1*, *Nup214-Abl1*, and *Ptpn1*), 7 (*Bcl7c*), 10 (*Tcf3*), and 19 (*Pten*).

LCC-Seq identified 28 deletions involving *Notch1* in 60 independent samples (Supplemental Table 7). Those deletions led to loss of *Notch1* exons 2, 1–2, 1–4, 1–19, 1–23, 1–24, 1–27, 3–27, 16–26, or 16–27 (Supplemental Table 7 and Figure 4A). Aberrant *Notch1* mRNA splice junctions were detected in samples that had deletions that retained exon 1 (Figure 4B and Supplemental Figure 8). Importantly, all the aberrant splice forms (loss of 3–27, 16–27) retained exon 28, which contains an alternate translation initiation site at *Notch1* M1727 (28). Western blot and RT-PCR indicated that samples with *Notch1* interstitial deletion produced an ICN protein and high *Hes1* expression (Figure 4, C and D).

To determine whether sustained high-level *Notch1* signaling was required for vigorous growth of the *Mcm2*$^{cre/cre}$ TCL, we treated *Notch1*-deleted cell lines with Compound E, a γ-secretase inhibitor that prevents cleavage of the membrane-bound ICN and resultant transport of the transcriptionally active ICN to the nucleus (26). Compound E did not affect growth of 2795 TCL, a cell line that was WT for *Notch1* (Supplemental Figure 9A) but significantly inhibited the growth and ICN expression of *Mcm2*$^{cre/cre}$ pre-T LBL cell lines with *Notch1* mutations (Supplemental Figure 9, B–F). These results indicated that *Mcm2*$^{cre/cre}$ TCLs require ongoing *Notch1* signaling for active proliferation in vitro.

Mcm2$^{cre/cre}$ *NHD13*$^{+}$ *mice develop BCP-ALL*. In addition to the pre-T LBL detected in the thymus, 12 of 46 *Mcm2*$^{cre/cre}$ *NHD13*$^{+}$ mice had an unexpected B cell expansion in the BM and spleen (Figure 5A and Supplemental Table 1). None of the *Mcm2*$^{cre/cre}$ *NHD13*$^{–}$ mice showed this phenotype, in which a predominant CD19^{+}B220$^{–/dim}$ or CD19$^{–}$B220^{dim} population was identified in the BM and spleen, while the thymus was infiltrated with CD4^{+}CD8^{+} pre-T LBLs (Figure 5A). Histological analysis showed infiltration of the BM, spleen, and kidney with clusters of B220^{+} cells; conversely, the thymus did not stain for B220 but stained for CD3 (Figure 5B), and BM was replaced with lymphoblasts (Figure 5C). The diagnosis of BCP-ALL was further supported by the presence of clonal *Igh* gene rearrangements (Figure 5D and Supplemental Table 8). In addition to BCP-ALL in *Mcm2*$^{cre/cre}$ *NHD13*$^{+}$ mice, 10% of *Mcm2*$^{cre/wt}$ *NHD13*$^{+}$ mice and 11% of *Mcm2*$^{wt/wt}$ *NHD13*$^{+}$ mice developed BCP-ALL (Figure 5E and Supplemental Table 8). The ratio of AML to BCP-ALL in *Mcm2*$^{cre/wt}$ *NHD13*$^{+}$ and *Mcm2*$^{wt/wt}$ *NHD13*$^{+}$ mice was 7:1 and 7:1, respectively, similar to previously published findings for NHD13 mice (14). However, the ratio of AML to BCP-ALL in the *Mcm2*$^{cre/cre}$ *NHD13*$^{+}$ mice was 0 because no *Mcm2*$^{cre/cre}$ *NHD13*$^{+}$ mice developed AML. The skewed proportion of BCP-ALL in *Mcm2*$^{cre/cre}$ *NHD13*$^{+}$ mice compared with *Mcm2*$^{wt/wt}$ *NHD13*$^{+}$ indicated that the *Mcm2* hypomorph dramatically accelerated the development of BCP-ALL, but not AML, in the NHD13^{+} background (Table 2).

To gain insight into the leukemic transformation of *Mcm2*$^{cre/cre}$ *NHD13*$^{+}$ B cell precursors, we assessed the differentiation of B and T cells from *Mcm2*$^{cre/cre}$ *NHD13*$^{+}$ mice at 1 month of age, before overt leukemic transformation. Flow cytometry showed a modest decrease in B220^{+}CD19^{+} precursors in *Mcm2*$^{wt/wt}$ *NHD13*$^{+}$ and *Mcm2*$^{cre/cre}$ *NHD13*$^{–}$ compared with WT mice; however, there was a marked decrease in B220^{+}CD19^{+} precursors in *Mcm2*$^{cre/cre}$ *NHD13*$^{+}$ BM, suggesting impaired B cell maturation. Subfractionation of B cell precursors revealed a 7-fold decrease (21% vs. 3%) of B220^{+}CD43$^{–}$ pre-B cells in the *Mcm2*$^{cre/cre}$ *NHD13*$^{+}$ BM, while the proportion of pro-B cells was similar in all 4 genotypes (Supplemental Figure 10, A–C), suggesting a block in differentiation at the pro-B to pre-B stage of maturation. In contrast, we detected no clear abnormalities of T cell differentiation at 1 month of age in any thymocyte or splenocyte of the genotypes studied (Supplemental Figure 10, D and E).

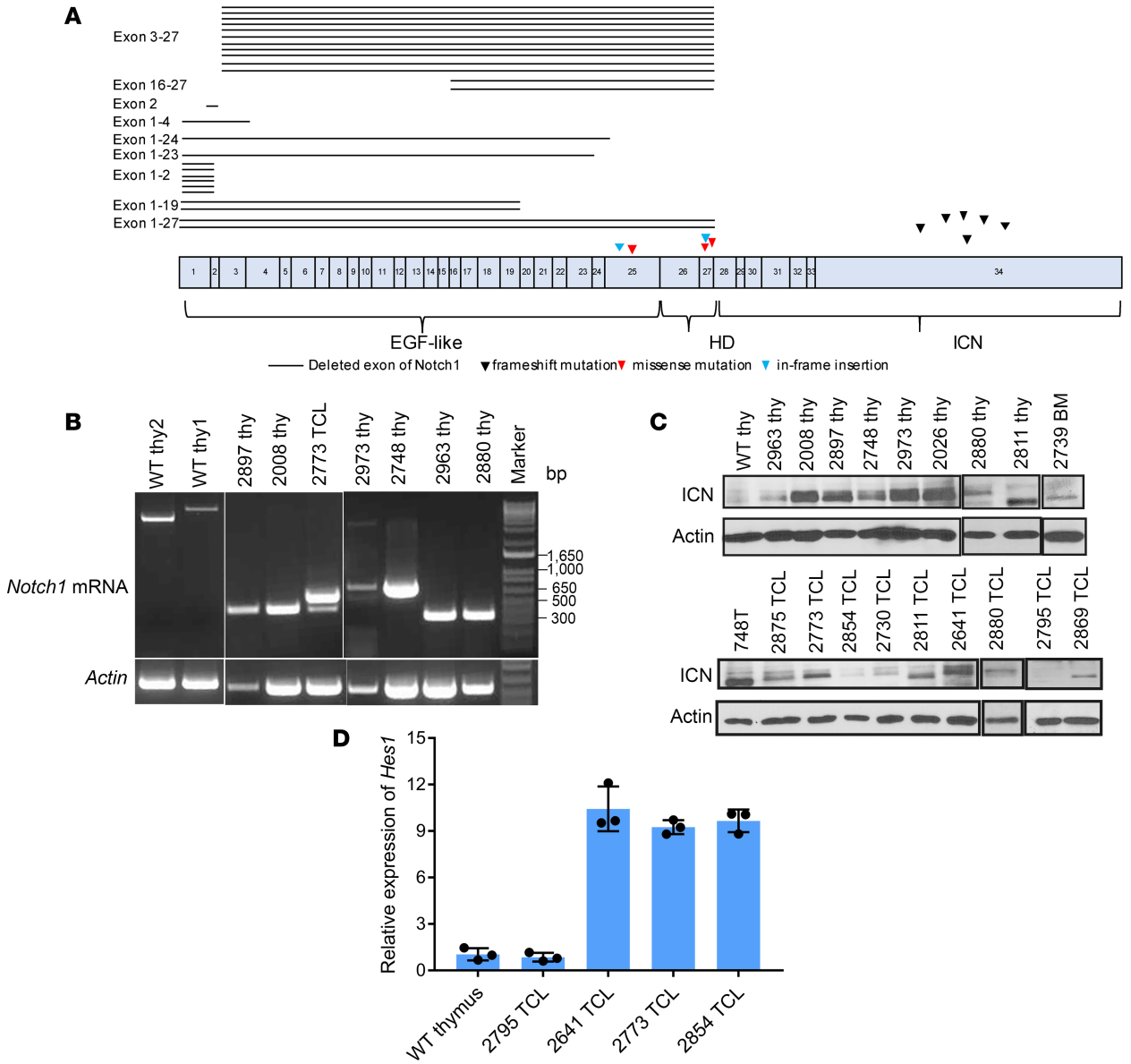

Figure 4. Interstitial deletions lead to activation of *Notch1*. (**A**) Summary of *Notch1* deletions. *Notch1* (ENSMUSG00000026923) exons are indicated in blue. Functional domains (EGF-like ligand-binding domain, HD, and intracellular domain of Notch1 [ICN]) as shown. Deleted exons of *Notch1*, frameshift mutations, missense mutations, and in-frame insertion are indicated. (**B**) Aberrant *Notch1* mRNA splice forms in 2880, 2963, 2748, 2973, 2008, and 2897 thymus and 2773 TCL. RT-PCR for WT (WT thy1), 2880, 2963, 2008, and 2897 thymus and 2773 TCL was performed by using primers located in exons 1 and 29 of *Notch1* to detect the junction of exon 2 and exon 28. RT-PCR for WT (WT thy2), 2748, and 2973 thymus was performed by using primers located in exons 13 and 29 of *Notch1* to detect the junction of exon 15 and exon 28. The lanes were grouped from different gels as indicated by the vertical lines. (**C**) ICN expression in pre-T LBL primary tumor and pre-T LBL cell line. The lanes were grouped from different gels as indicated by the vertical lines. (**D**) RT-PCR analysis of Notch1 target *Hes1* expression in WT thymus and pre-T LBL with *Notch1* mutations. Error bars represent standard deviation of 3 technical replicates (n = 3).

Recurrent CNAs in BCP-ALL. Similar to pre-T LBL samples, we identified recurrent acquired CNAs in $Mcm2^{cre/cre}$ $NHD13^{+}$ BCP-ALL (Figure 6A and Supplemental Figure 11A). We also assessed CNAs in 4 $Mcm2^{cre/wt}$ $NHD13^{+}$ samples; as opposed to the pattern of 125–1000 kb deletions seen in $Mcm2^{cre/cre}$ malignancies (both pre-T LBL and BCP-ALL), there were few 125–1000 kb deletions in the $Mcm2^{cre/wt}$ $NHD13^{+}$, consistent with prior observations that mice heterozygous for an $Mcm2^{cre}$ allele are not prone to the deleter phenotype. Comparison of CNAs from pre-T LBL and BCP-ALL from the same mouse showed no similarities between the pairs (Supplemental Figure 11, B–D), indicating that the T and B cell malignancies did not arise from a common precursor.

Five of 7 $Mcm2^{cre/cre}$ $NHD13^{+}$ BCP-ALLs showed deletion involving *Pax5*, one of the most frequently mutated genes in human BCP-ALL (Figure 6B and Supplemental Table 9). Moreover, the same 5 samples showed deletion (4 of 5 homozygous) of a region that encompassed *Cebpb* and *Ptpn1* (Figure 6, C and D,

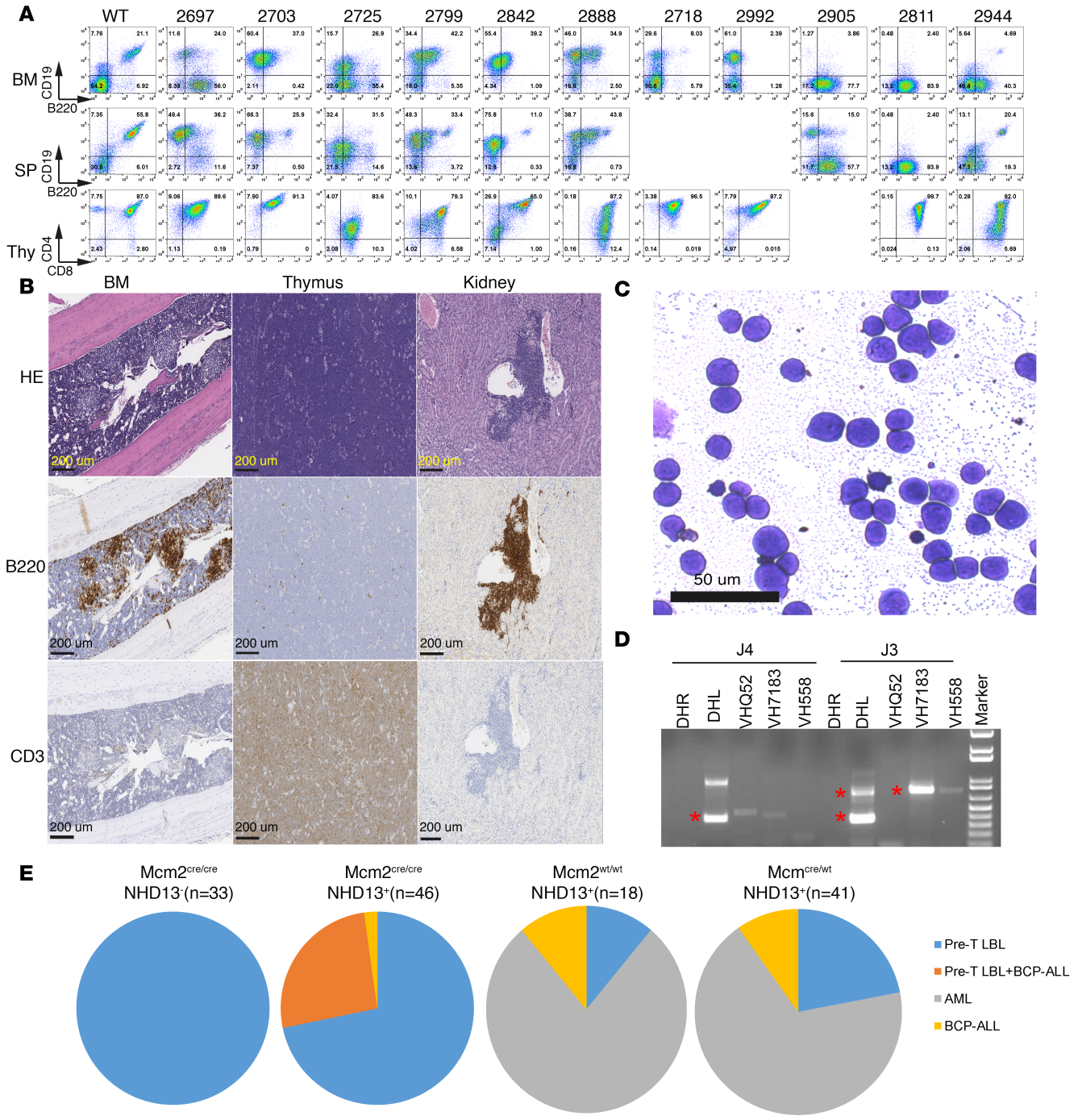

Figure 5. *Mcm2*$^{cre/cre}$ *NHD13*$^{+}$ mice develop BCP-ALL. (**A**) Flow cytometry plots of BM and spleen (SP) stained with CD19 and B220 and thymocytes (thy) stained with CD4 and CD8 from *Mcm2*$^{cre/cre}$ *NHD13*$^{+}$ mice with BCP-ALL. WT BM, SP, and Thy are controls. (**B**) Hematoxylin and eosin (H&E) and B220 and CD3 IHC of infiltrated BM, thymus, and kidney of mouse 2725 with concurrent BCP-ALL and pre-T LBL. Scale bar: 200 μm. (**C**) May-Grünwald-Giemsa–stained BM lymphoblasts from a mouse with BCP-ALL (number 2811). Scale bar: 50 μm. (**D**) *Igh* gene rearrangement assay for 2697 BM; clonal fragments indicated by a red asterisk were sequenced. (**E**) Frequency of leukemia subtypes by genotype (*Mcm2*$^{cre/cre}$ *NHD13*$^{-}$ [*n* = 33], *Mcm2*$^{cre/cre}$ *NHD13*$^{+}$ [*n* = 46], *Mcm2*$^{wt/wt}$ *NHD13*$^{+}$ [*n* = 18], and *Mcm2*$^{cre/wt}$ *NHD13*$^{+}$ [*n* = 41]).

and Supplemental Table 9). However, *Cebpb* is not highly expressed in normal B cell precursors, whereas *Ptpn1* is highly expressed in B cell precursors. Figure 6E shows marked downregulation of *Ptpn1* in 4 samples with putative homozygous deletions.

Recurrent Nup214-Abl1 fusion gene in Mcm2$^{cre/cre}$ *NHD13*$^{+}$ *BCP-ALL.* Four *Mcm2*$^{cre/cre}$ *NHD13*$^{+}$ BCP-ALLs showed copy number gain (estimated 1–2 copies) of a region bounded by *Abl1* and *Nup214* (Figure 7A and

Table 2. Total number of AMLs and BCP-ALLs in mice with indicated genotype

	Mcm2$^{wt/wt}$ *NHD13*$^{+}$	*Mcm2*$^{cre/wt}$ *NHD13*$^{+}$	*Mcm2*$^{cre/cre}$ *NHD13*$^{+}$
AML	14	28	0
BCP-ALL	2	4	12
P value[A] (vs. *Mcm2*$^{wt/wt}$ *NHD13*$^{+}$)	N/A	1	0.00001

[A]Calculated by Fisher's exact test.

Supplemental Table 9). Given that *NUP214-ABL1* fusions have been identified in patients with pre-T LBL (31) and BCP-ALL (32), we hypothesized that *Nup214-Abl1* gains could result in a *Nup214-Abl1* fusion. This putative fusion could be produced by an episome, as shown in human pre-T LBL (31), or by a tandem duplication (Figure 7B). We designed primers to amplify a fusion between *Nup214* exon 23, 29, 31, 32, or 34 and *Abl1* exon 2 based on the fusions in human pre-T LBL (31). A fusion PCR product was identified in all 4 samples that showed *Nup214-Abl1* copy number gain (samples 2842, 2811, 2725, and 2703). In addition, a *Nup214-Abl1* fusion was identified in 1 sample (sample 2905) that did not show an amplified region and in 2 of 3 samples that were not assayed for CNAs (Figure 7C). *Nup214-Abl1* fusion genes were not identified in pre-T LBL, AML, or *Mcm2*$^{cre/wt}$ *NHD13*$^{+}$ BCP-ALL (Figure 7, C and D). Nucleotide sequencing demonstrated a *Nup214* exon 32 to *Abl1* exon 2 fusion in 6 samples; 1 sample (sample 2697) had a *Nup214* exon 31 to *Abl1* exon 2 fusion (Table 3). *Crkl*, a direct target of the *Abl1* kinase (31), was phosphorylated in splenocytes that expressed the *Nup214-Abl1* fusion (Figure 7E), indicating that *Nup214-Abl1* acts as an activated *Abl1* kinase. Imatinib, an inhibitor of Abl1 kinase (33), inhibited the growth of splenocytes, which expressed a *Nup214-Abl1* fusion (Figure 7F).

We used WES to identify Tier 1 (coding) mutations in *Mcm2*$^{cre/cre}$ *NHD13*$^{+}$ mice and found no recurrent mutations in the 11 samples assayed (Supplemental Table 10). In contrast, all 3 *Mcm2*$^{cre/wt}$ *NHD13*$^{+}$ samples showed at least 1 Tier 1 mutation in genes known to be relevant for human BCP-ALL (*Sh2b3* [ref. 34], *Jak1*, *Trp53*, or *Flt3* [ref. 35]) (Supplemental Table 10 and Supplemental Figure 12).

Nucleotide-level resolution of deletion breakpoints. As seen in Figure 2, the genomic regions most susceptible to the 10–1000 kb deletions triggered by the *Mcm2* hypomorph are not random but occur within a limited number of regions. To determine whether the breakpoint junctions are focal and follow any clear rules or patterns (such as VDJ recombination), we used LCC-Seq to capture and analyze the breakpoints of several selected regions (*Pten*, *Notch1*, *Tcf3*, *Bcl7c*, *Ptpn1*, and *Nup214-Abl1*) at a nucleotide level. In total, we identified 245 deletions in 91 samples (Supplemental Table 11). Identical deletions found in primary tumor and cell lines were considered a single independent event. Detailed analysis of the sequence at the deletion junction of 245 independent deleted regions revealed that 155 of the 245 junctions had 1–7 bp of microhomology (Supplemental Table 11). Seventy junctions contained nontemplated insertions at the breakpoint junctions; some of these were quite extensive, 1–54 nucleotides in length. Given the precedent set by programmed VDJ rearrangement, in which signal sequences can occur at a distance (up to 38 bp) from the breakpoint junction, we analyzed nucleotide sequences in a 200-bp window (100-bp 5′ and 100-bp 3′) flanking both the upstream and downstream breakpoints, in both the WGS data set (Supplemental Table 4) and the LCC-Seq data set (Supplemental Table 11). Comparison of 156 windows from the WGS to 7332 randomly selected 200-bp windows revealed an increased likelihood of mononucleotide repeats in the Mcm2 tumor breakpoints identified by WGS ($P = 0.009456$; Supplemental Figure 13A and Supplemental Tables 12 and 13). Moreover, comparison of 490 windows from the 245 independent breakpoints identified by LCC-Seq with 7530 randomly selected 200-bp windows from chromosomes 2, 7, 10, and 19 (corresponding to the LCC-Seq chromosomes) also showed an increased frequency of mononucleotide repeats in the Mcm2 tumor breakpoints ($P = 0.009671$; Supplemental Figure 13B and Supplemental Tables 14 and 15). These findings are consistent with the observation that upon replication stress, DNA breaks are frequently generated at mononucleotide repeats (36).

Discussion

Replication stress has been linked to many forms of cancer (1, 3). It has been speculated that replicative stress leads to DNA DSBs, with subsequent repair by non-homologous end joining (NHEJ), resulting in indel mutations and structural variations, including large interstitial deletions. It is thought that these mutations, such as deletions of important tumor suppressor genes, ultimately cause malignancy. These frequent DNA

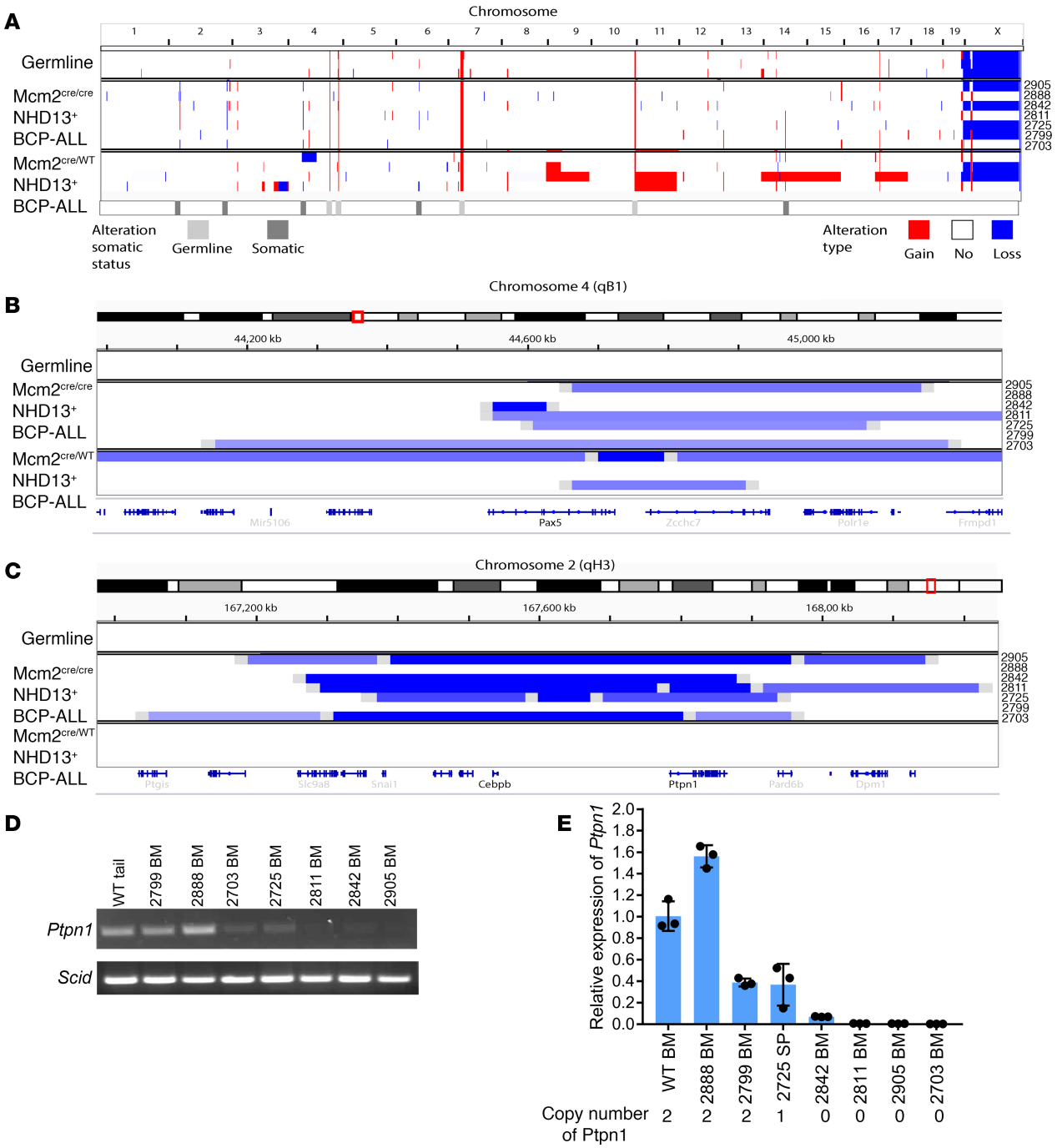

Figure 6. CNA analysis of BCP-ALL. (**A**) CNA analysis of germline and BCP-ALL (*Mcm2*$^{cre/cre}$ *NHD13*$^{+}$ [*n* = 7] and *Mcm2*$^{cre/wt}$ *NHD13*$^{+}$ [*n* = 4] mice); samples were more than 60% tumor tissue (BM) based on flow cytometry. The IDs of *Mcm2*$^{cre/cre}$ *NHD13*$^{+}$ mice are indicated on the right side. Color code as in Figure 2A. (**B** and **C**) CNAs for *Pax5* region (**B**) and *Cebpb/Ptpn1* region (**C**). Color code as in Figure 2A. (**D**) PCR amplification of *Ptpn1*-deleted region. Faint signals in 2703 and 2725 could be due to haploinsufficiency or contamination with nonmalignant cells. (**E**) *Ptpn1* mRNA expression, samples, and copy number of *Ptpn1* (CNAs) are indicated. Error bars represent standard deviation of 3 technical replicates (*n* = 3). mRNA expression is markedly decreased in samples with 2 copies lost.

DSBs caused by increased replicative stress lead to activation of Chk1; Chk1 inhibitors have recently entered the clinic (37) as an approach to target unique vulnerabilities in the cancer cell. In this study, we show that mutation of a single gene (*Mcm2*) leads to a deleter phenotype and that resultant combinations of deletions involving several critical genes act in concert and are selected in vivo as T or B lymphoid malignancies.

Hypomorphs of several members of the Mcm2–7 DNA replicative helicase complex show malignancy or stem cell defects (9, 38–40), which is thought to be associated with replicative stress; in some cases,

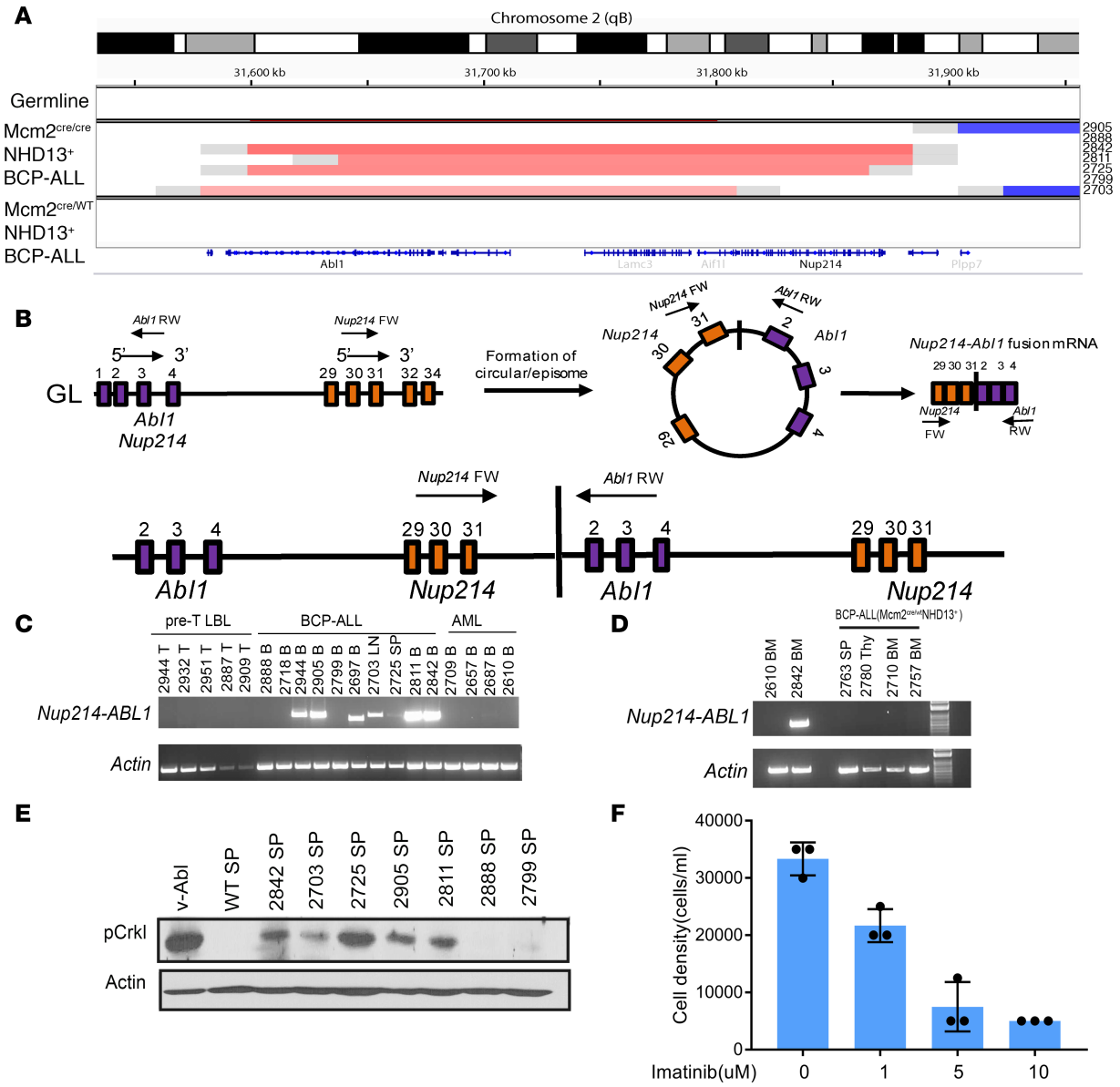

Figure 7. Recurrent *Nup214-Abl1* fusion gene detected in BCP-ALL. (**A**) CNAs for the *Abl1*- and *Nup214*-containing region of chromosome 2. Color code as in Figure 2A. (**B**) Schematic for putative *Nup214-Abl1* fusion gene produced via episome or tandem duplication. (**C**) RT-PCR detection of *Nup214-Abl1* fusion mRNA using *Nup214* exon 29 forward primer and *Abl1* exon 2 reverse primer. Pre-T LBL samples are from mice with genotype $Mcm2^{cre/cre}$ $NHD13^{+}$ and $Mcm2^{cre/cre}$ $NHD13^{-}$, BCP-ALL samples are from mice with genotype $Mcm2^{cre/cre}$ $NHD13^{-}$, and AML samples are from mice with genotype $Mcm2^{cre/wt}$ $NHD13^{+}$. B, bone marrow; T, thymus; LN, lymph node; SP, spleen. (**D**) RT-PCR does not show *Nup214-Abl1* fusion mRNA in BCP-ALL from $Mcm2^{cre/wt}$ $NHD13^{+}$ mice; 2842 is a positive control. (**E**) Phosphorylation of Crkl in the spleen of mice (WT, 2842, 2703, 2725, 2905, 2811, 2888, and 2799) with *Nup214-Abl1* fusion; *v-Abl* transformed B cell line is a positive control. (**F**) Imatinib treatment inhibited the growth of 2725 splenocytes that expressed a *Nup214-Abl1* fusion. Growth curves of 2725 splenocytes treated with imatinib for 2 days. Cell number was counted by trypan blue exclusion. Error bars represent standard deviation of 3 technical replicates (n = 3).

these malignancies were linked to recurrent interstitial deletions (7, 9, 41). We reasoned that tumor suppressor genes that are important for transformation of MDS to AML could be identified by crossing the *Mcm2* mice with a deleter phenotype to *NHD13* mice. However, all $Mcm2^{cre/cre}$ $NHD13^{+}$ developed T and/or B cell malignancies, but not AML, within 5 months of age. We also predicted that $Mcm2^{cre/wt}$ mice, which express approximately 30%–40% less Mcm2 protein than WT mice, might have a subtle predisposition to malignancy that can be revealed by a cooperating oncogenic event (such as the *NHD13* transgene). However, although $Mcm2^{cre/wt}$ $NHD13^{+}$ developed AML, the incidence, age of onset, and immunophenotype was similar to $Mcm2^{wt/wt}$ $NHD13^{+}$ (Figure 1A), suggesting that a single copy of the $Mcm2^{cre}$ allele did not predispose to AML. Furthermore, CNA showed that the $Mcm2^{cre/wt}$ $NHD13^{+}$ AML samples did not have

Table 3. Sequence of *Nup214-Abl1* fusion junctions

ID	*Nup214*ex32-*Abl1*ex2	*Nup214*ex31-*Abl1*ex2
2905	**CAAATAAAACAG**AAGCCCTGCA	
2697		**GCTGCCCCAA**AAGCCCTGCA
2811	**CAAATAAAACAG**AAGCCCTGCA	
2725	**CAAATAAAACAG**AAGCCCTGCA	
2703	**CAAATAAAACAG**AAGCCCTGCA	
2842	**CAAATAAAACAG**AAGCCCTGCA	
2944	**CAAATAAAACAG**AAGCCCTGCA	

Bold font represents the Nup214 sequence of the *Nup214-Abl* fusion whereas nonbold font represents the *Abl1* sequence.

recurrent deletions, reinforcing the idea that $Mcm2^{cre/wt}$ mice are not predisposed to malignancy. Although it was previously shown that $Mcm2^{cre/wt}$ mice are not prone to recurrent deletions (9), it remains possible that $Mcm2^{cre/wt}$ mice are prone to more infrequent deletions that are not evident because they are polyclonal and not discernable in a polyclonal population of cells. However, the observation that clonal $Mcm2^{cre/wt}$ $NHD13^{+}$ AML samples did not show deletions argues strongly against that possibility. Given that all $Mcm2^{cre/cre}$ $NHD13^{+}$ mice died of pre-T LBL or BCP-ALL by 5 months of age, it remains possible that these mice did not develop AML because they died before AML had a chance to develop.

There were 4–32 deletions per tumor. Nucleotide sequence analysis revealed that there was an increased likelihood of mononucleotide repeats at or near the deletion breakpoints, consistent with the hypothesis that polymerase pausing or stalling at sites of mononucleotide repeats leads to DNA DSBs (42, 43); improper repair of 2 such breaks via NHEJ leads to the interstitial deletions. Given that studies of human pre-T LBL have suggested that there may be 2–4 "driver" mutations per tumor (24), we considered that many of the deletions were likely to be passenger deletions. Recurrent deletions may still be passenger deletions in this model, selected by virtue of susceptibility to deletion. Some regions had numerous homozygous deletions, centered over a single gene, such as *Pten*. Alternatively, there were regions where the individual deletions were spread over a larger 2–3 Mb region, with no clear common deleted region, and few homozygous deletions, such as the region encompassing *Bcl7a*. We suspect the former are more likely to be driver deletions and the latter more likely to be passenger deletions. Using these criteria, the leading candidates for driver deletions were *Pten* and *Tcf3*. These candidates are supported by experimental studies that show homozygous *Pten* and *Tcf3* deletions strongly predispose mice to pre-T LBL (21, 44). Moreover, *PTEN* deletions/mutations are quite common in human pre-T LBL (16%, ref. 20). In addition, although *TCF3* deletions are uncommon in human pre-T LBL, enforced expression of *TAL1* by a large variety of genomic rearrangements is quite common (24); in this context, it is important to note that enforced expression of *TAL1* leads to a functional inactivation of *TCF3* (45). Of note was a significantly increased likelihood of *Dnmt3a* mutations, especially homozygous *Dnmt3a* mutations (3/11 vs. 0/18; $P = 0.0096$), in $Mcm2^{cre/cre}$ $NHD13^{-}$ mice compared with the $Mcm2^{cre/cre}$ $NHD13^{+}$ mice. A plausible explanation for this observation is that NUP98 fusion proteins have been shown to increase stem cell self-renewal (46), as has *Dnmt3a* deletion (47). Thus a homozygous *Dnmt3a* deletion that promotes stem cell self-renewal may be redundant in the context of an $NHD13^{+}$ cell that also leads to increased self-renewal potential.

Notch1 deletions represent a special case in terms of thymocyte transformation. In contrast to *Pten* and *Tcf3*, in which homozygous deletion of the genes predisposes to pre-T LBL, *Notch1* mutations are most commonly monoallelic point mutations of the HD or PEST domain in both humans and mice (26, 27). Mutations in the HD lead to loss of requirement for extracellular Notch1 ligand binding, and PEST domain mutations result in decreased degradation of the transcriptionally active ICN, resulting in sustained activation of Notch1 target genes (26). A recurrent interstitial deletion of *Notch1* exons 1–2 leads to translation initiation at an internal methionine residue (M1727), production of a protein that lacks the extracellular domain, and ligand-independent activation of Notch1 (28). In this study, we show recurrent *Notch1* genomic deletions removed the Notch1 extracellular domain and retained the transcriptionally active ICN.

Consistent with the notion that driver mutations were produced by recurrent interstitial deletions in this model, WES studies showed relatively few SNVs or indels. The only recurrent Tier 1 mutations identified in 29 samples were 4 *Notch1*, 1 *Ezh2*, and 2 *Tp53* mutations. These results stand in contrast to our prior WES studies of murine leukemia and lymphoma on a WT *Mcm2* background, in which

60%–100% of malignancies had acquired Tier 1 mutations in genes known to be mutated in hematological malignancy (48, 49).

Serial analysis of the *Mcm2*$^{cre/cre}$ pre-T LBL cell lines suggests that the *Notch1* mutations are relatively late events, consistent with sequencing studies of human pre-T LBL, in which almost half the *Notch1* mutations identified were thought to be subclonal (24). An overall scheme for cooperative lesions that result in transformation in this model is outlined in Supplemental Figure 14A. Increased stem cell self-renewal is conferred by either the *NHD13* transgene or *Dnmt3a* inactivation. *Tcf3* deletion results in a block to thymocyte differentiation, and *Pten* deletion leads to hyperproliferation. Finally, *Notch1* mutations lead to ligand-independent growth; the cells no longer require Notch1 ligands supplied by thymic epithelial cells and are able to metastasize as well as expand in vitro.

CNA analysis of pre-T LBL cell lines indicated that the overall frequency of new deletions seemed to decrease with time (Table 1). The decreased frequency of new deletions could reflect accommodation to the Mcm2 protein deficiency; alternatively, it is conceivable that there are relatively few exquisitely sensitive regions susceptible to deletion in *Mcm2* hypomorph pre-T LBL, and these are deleted relatively early. The ongoing Mcm2 deficiency suggests that these cell lines could be useful for the study of Mcm2 biology or evolutionary pressures in cancer. For instance, CNA analysis of cell lines selected for resistance to clinically relevant chemotherapy agents (for instance, vinca alkaloids or alkylating agents), could be used to identify genes and pathways important for this acquired resistance.

Approximately 26% of *Mcm2*$^{cre/cre}$ *NHD13*$^{+}$ developed concurrent BCP-ALL and pre-T LBL. CNA analysis of BCP-ALL was in general simpler than the pre-T LBL, with fewer deletions per sample. *Pax5* and *Ptpn1* were recurrently deleted, and these deletions were invariably accompanied by *Nup214-Abl1* fusion similar to that seen in a subset of human pre-T LBL and BCP-ALL (31, 32). The *Nup214-Abl1* fusions were functional, as shown by Crkl phosphorylation and sensitivity to imatinib. WES showed no recurrent Tier 1 SNVs, consistent with the notion that driver mutations in *Mcm2* hypomorph mice were primarily CNAs. Taken together, the complementary pathways involved in this model match those predicted for human BCP-ALL (50). In this context, the collaborative pathways and genes are: (a) increased stem cell self-renewal conferred by the *NHD13*$^{+}$ transgene, (b) impaired B cell differentiation caused by *Pax5* deletion, and (c) hyperproliferation conferred by a *Nup214-Abl1* fusion gene (Supplemental Figure 14B). Although the role of *Ptpn1* deletion is unclear, it is interesting to note *Ptpn1* deletion accelerates lymphoma onset in *Trp53*-deficient mice (51), conceivably by enforcing active kinase signaling (52), and deletions of the closely related *PTPN2* are common in pre-T LBL patients with *NUP214-ABL1* fusion. In both cases, the *PTPN* deletion is thought to be oncogenic through enforcing hyperactive kinase signaling (52, 53).

Taken together, these findings demonstrate that replicative stress can result in cancer through the generation of chromosomal rearrangements, most commonly interstitial deletions of about 50–1000 kb. The genetic lesions selected in vivo (*Dnmt3a*, *Pten*, *Tcf3*, and *Notch1* for pre-T LBL and *Pax5* and *Abl1* for BCP-ALL) are frequent events in the corresponding human lymphoid leukemias, reinforcing the idea that collaborative pathways leading to lymphoid leukemias are similar between mice and humans. Combinations of CNAs involving tumor suppressor genes or oncogenes are selected because of fitness advantage and provide an in vivo mammalian model for evolution and selection within a time frame of months.

Methods

Mice and genotyping

Mcm2$^{cre/cre}$ and *NHD13*-transgenic mice were generated as previously reported; congenic *Mcm2* on a C57BL/6 background mice were generated as described previously (6, 9, 14). The genotyping of *NHD13* and *Mcm2* mice was performed as previously described (6, 9, 14) with primers listed in Supplemental Table 16. CBCs were performed on peripheral blood using a HEMAVET Multispecies Hematology Analyzer (CDC Technologies). Diagnosis of hematological malignancy was based on previously published consensus guidelines (54).

Flow cytometry, IHC, and immunoblots

Flow cytometry was performed as described previously (29) with the following antibodies: from eBioscience: Mac1 (CD11b)-PE (catalog 12-0112-82), CD4-PE (catalog 12-0043-82), Gr1-FITC (catalog 11-5931-85), Ter119-FITC (catalog 11-5921-85), c-Kit (CD117)-FITC (catalog 11-1171-82), CD43-FITC (catalog 11-0431-82), CD44-FITC (catalog 11-0441-82), CD25-PE (catalog 12-0251-82), CD4-APC (catalog 17-0042-82), and

CD8-APC-780 (catalog 47-0081-82); and from BD Biosciences: CD8-FITC (catalog 553031), CD71-PE (catalog 553267), Sca-1-PE (catalog 553108), B220 (CD45R)-FITC (catalog 553088), and CD19-PE (catalog 553786). IHC and immunoblotting were performed as previously described (29). Formalin-fixed, paraffin-embedded tissue sections were stained with H&E, myeloperoxidase (A0398; Dako), CD3 (MCA1477; Bio-Rad), and B220 (553086; BD Biosciences). Stained sections were scanned and imaged as previously reported (29). For immunoblots, proteins were separated by 7.5% SDS-PAGE (Bio-Rad Laboratories) and transferred to nitrocellulose membranes (Thermo Fisher Scientific). Primary antibodies used were anti-Mcm2 (610701, Trans-duction Laboratories), anti-PTEN (D4.3) XP (9188, Cell Signaling Technology), anti–phospho-Crkl (Tyr207) (181, Cell Signaling Technology), anti–cleaved Notch1 (Val1744) (D3B8) (4147, Cell Signaling Technology), anti–β-actin (A5316, MilliporeSigma), and anti–α-tubulin (2125S, Cell Signaling Technology). After application of appropriate secondary antibodies conjugated to HRP (goat anti-mouse, 31430; and goat anti-rabbit, 31460, both from Thermo Fisher Scientific), signals were visualized using Pierce ECL Western Blotting Substrate (Thermo Fisher Scientific) and Amersham Hyperfilm ECL (GE Healthcare Ltd.).

Cell culture and cell lines

Pre-T LBL (2875, 2854, 2880, 2730, 2773, 2696, 2795, 2869, 2883, 2641, 2739, and 2973 TCL) cell lines were established from single-cell suspensions prepared from thymus (1×10^6 cells) of sick mice and maintained in IMDM supplemented with 15% FBS, 100 mmol/L L-glutamine, and 100 μg/mL penicillin/streptomycin (Invitrogen, Thermo Fisher Scientific) without supplemental cytokines. Splenocytes from mouse 2725 that expressed a *Nup214-Abl1* fusion were maintained in RPMI 1640 medium (Gibco, Thermo Fisher Scientific) supplemented with 10% heat-inactivated FBS, 1 mM L-glutamine, 100 U/mL streptomycin, 100 μg/mL penicillin, 50 μM 2-ME (all from Gibco, Thermo Fisher Scientific), and 10 ng/mL IL-7 (217-17; Peprotech).

Assessment of Compound E and imatinib mesylate treatment

Compound E (ALX-270-415, Enzo Life Science) was dissolved in DMSO and evaluated at a final concentration of 1 μM. Pre-T LBL cell lines (5×10^4 /mL) were seeded in IMDM supplemented with 15% FBS, 100 mmol/L L-glutamine, and 100 μg/mL penicillin/streptomycin. The cells were treated with 1 μM Compound E or vehicle (DMSO) only for 4 days, and cell number was determined by trypan blue exclusion daily (TC20 Automated Cell Counter, Bio-Rad Laboratories, Inc). Imatinib mesylate (S1026, Selleckchem) was dissolved in DMSO and evaluated at 1, 5, and 10 μM. Splenocytes from mouse 2725 (5×10^4 /mL) were seeded in RPMI 1640 medium supplemented with 10% heat-inactivated FBS, 1 mM L-glutamine, 100 U/mL streptomycin, 100 μg/mL penicillin, 50 μM 2-ME, and 10 ng/mL IL-7. The cells were treated with imatinib mesylate or vehicle only for 4 days, and cell number was determined by trypan blue exclusion daily.

PCR and Sanger sequencing

Genomic DNA was extracted with the DNeasy Blood & Tissue (QIAGEN) kit according to the manufacturer's recommended protocol. PCR was performed using HiFi Taq polymerase mix (10790-020; Invitrogen, Thermo Fisher Scientific) and primers (Invitrogen, Thermo Fisher Scientific) as listed in Supplemental Table 16. Clonal *Igh* and *Tcrb* DJ or VDJ segments were identified using previously described PCR-based assays (29) with primers listed in Supplemental Table 16. RNA was extracted using TRIzol (Invitrogen, Thermo Fisher Scientific) and the manufacturer's recommended protocol. cDNA was synthesized by reverse transcriptase using 1 μg RNA with SuperScript III enzyme and reagents (Invitrogen, Thermo Fisher Scientific). cDNA splice sites for *Notch1*, *Ikzf1*, and *Nup214-Abl1* were identified by PCR amplification of cDNA and confirmed by Sanger sequencing. Selected mutations identified by WES or LCC-Seq were PCR amplified, purified, and confirmed by Sanger sequencing. Real-time quantitative PCR was performed with a *Ptpn1* TaqMan primer probe (Mm00448427_m1, Thermo Fisher Scientific) and *Hes1* TaqMan primer probe (Mm01342805_m1, Thermo Fisher Scientific) sets and ABI Fast Universal PCR Master Mix on the ABI Fast7500 system (Applied Biosystems, Thermo Fisher Scientific). Samples were normalized to endogenous 18S rRNA with TaqMan Ribosomal RNA Control Reagents. Sanger sequencing was performed at the National Cancer Institute Sequencing Minicore facility.

Sparse WGS for CNAs

Preparation of genomic libraries for sparse WGS was performed as previously described (19). In brief, 1 μg of genomic DNA was sonicated using the Covaris instrument followed by end repair and A-tail addition. TruSeq dual index adapters were subsequently ligated to DNA molecules, with ligated products

enriched via PCR amplification. Indexed libraries were pooled and sequenced in multiplex fashion while targeting about 4 million reads per sample. Data analysis was performed as described previously (55) with the exception that new higher resolution bin boundaries were constructed to facilitate the analysis. Specifically, mouse genome build mm9 was divided into 120,000 bins, while accounting for unique mappability. This allowed analysis of the CNAs at a segment resolution of about 125 kb (5 consecutive bins for segmentation) and breakpoint resolution of about 25 kb (average width of each bin).

WES, WGS, and LCC-Seq and sequencing analysis

Library preparation. Sequencing libraries were prepared through tagmentation using the Nextera DNA Library Kit (Illumina, Inc.) according to the manufacturer's instructions with the following modifications. PCR primers in the kit were replaced with i5 primer (5′-AATGATACGGCGACCACCGAGATCTACACNNNNNNNNTCGTCGGCAGCGTC-3′) and i7 primer (5′-CAAGCAGAAGACGGCATACGAGATNNNNNNNNGTCTCGTGGGCTCGG-3′), at a final concentration of 50 nM, where the Ns represent standard Nextera index sequences. Exome and Targeted Genomic CaptureExome capture was carried out using the SureSelect XT Mouse All Exon, 49.6 Mb Kit (Agilent Technologies, Inc.) following the manufacturer's protocol. BAC clones tiling the genomic regions of interest (Supplemental Table 17) were obtained (BACPAC Resources Center), and DNA was prepared using the QIAGEN Large-Construct Kit. BACs were pooled and capture bait prepared using biotinylated random hexamers and Klenow enzyme in a random primed extension reaction. Bait coupled to streptavidin magnetic beads was hybridized to library pools for 24 hours followed by stringency washes and PCR using primers homologous to the outermost adapter sequences of the sequencing libraries (5′-AATGATACGGCGACCACC-3′ and 5′-CAAGCAGAAGACGGCATA-3′). Sequencing Captured libraries were quantified by quantitative PCR (KAPA Biosystems) and sequenced on a HiSeq 2500 System (Illumina, Inc.).

Sequencing analysis. Data processing and variant calling procedure followed the Best Practices workflow recommended by the Broad Institute (56, 57). Briefly, the raw sequencing reads were mapped to mouse genome build 10 (mm10) by the Burrows-Wheeler Aligner (58) followed by local realignment using the GATK suite (59) from the Broad Institute, and duplicated reads were marked by the Picard tools (http://broadinstitute.github.io/picard).

Somatic variant calling was performed by comparison of tumor to WT samples using the MuTect2 (60) somatic variant caller in the GATK suite. SnpEff (61) variant annotation and effect prediction tool and dbSNP 137 (National Center for Biotechnology Information) were used to annotate and predict effects of the variants. LUMPY (62) was used for structural variant discovery in the WGS and LCC-Seq.

These were the filtering criteria for the somatic variants in the WES data: variants were first filtered with the GATK recommended filtering criteria (https://software.broadinstitute.org/gatk/documentation/article.php?id=3225 under "Filtering Recommendations") and then filtered with the following additional filters: (a) minimum fraction of altered reads in a tumor is 0.3; (b) minimum number of altered reads in a tumor is 2; (c) minimum log_fisher is 0.2; (d) impact effect is "High" or "Moderate" for Tier 1 indels and missense mutations; and (e) exclude SNPs reported in dbSNP build 137 or previously identified as germline variants in the NIH C57BL/6 colony.

These were the filtering criteria for the structure variants in the WGS data: (a) ALT = DEL; (b) SVLEN ≤ 1000; (c) normal AO = 0; and (d) manual check if deletions were present in the BAM files.

These were the filtering criteria for the structural variants (SVs) in the LCC-Seq data: (a) only keep SVs overlapping the bait regions; (b) maximum number of altered reads in the WT sample is 4; (c) minimum fraction of altered reads in a tumor is 0.1; and (d) manual check if deletions were present in the BAM files. Primary next-generation sequencing data are available at the National Center for Biotechnology Information's Sequence Read Archive, accession numbers PRJNA565491, PRJNA565494, PRJNA589636, and PRJNA565492.

Analysis of repeat sequences associated with tumor breakpoints

The breakpoints mapped in recurrent deletions using WGS and LCC-Seq are extended 100 bp on either side — 100 bp into the deletion and 100 bp into the region intact in the tumor. Each deletion is associated with 2 breakpoints. The DNA sequence of this 200-bp window was obtained using *bedtools getfasta* command (63). Tandem Repeat Finder was used to locate the mononucleotide repeat sequences around each breakpoint (64).

For each data set (WGS and LCC-Seq), a random data set of a 200-bp window was generated using *bedtools shuffle-chrom* command to maintain a similar chromosome distribution of the random data set as the tumor deletion data set (63). The DNA sequence and repeat sequence were mapped as explained earlier.

For the tumor deletion and random data set, the enrichment of mononucleotide repeats was evaluated using Fisher's Exact Test for Counts Data using R. The tumor deletion data set showed a significant enrichment of mononucleotide repeats with respect to the random data set.

Statistics

Data are displayed as mean ± standard deviation. Significance values were calculated using Student's *t* test (unpaired, 1-tailed distribution) in Microsoft Excel. The number of independent experiments, statistical tests, and *P* values are indicated in figure legends. Survival was analyzed using GraphPad Prism 7.01 software and log-rank (Mantel-Cox) test. $P < 0.05$ was considered significant.

Study approval

All studies involving mice were approved by the National Cancer Institute (Bethesda) Intramural Animal Care and Use Committee and were performed according to protocols approved by the National Cancer Institute (Bethesda) Intramural Animal Care and Use Committee.

Author contributions

MY, PDA, and SCP conceived and designed the project. MY, TB, RLW, SWL, and PDA developed the methods. MY, TB, RLW, SWL, AF, and TM performed experiments. MY, TB, YJZ, SS, AN, PSM, and PDA analyzed the data. MY wrote the initial draft of the manuscript. MY, TB, SCP, AN, TM, YJZ, SS, RLW, SWL, PSM, and PDA reviewed and edited the manuscript.

Acknowledgments

The authors thank current and former members of the Aplan lab for insightful discussions. We also thank the Cold Spring Harbor Laboratories sequencing facility, the NCI Sequencing Minicore for Sanger sequencing, the NCI Transgenic Core for generation of transgenic mice, the NCI Flow cytometry core for cell sorting, Maria Jorge for excellent animal husbandry, and Shelley Hoover, Mark Simpson, and Jennifer E. Dwyer of the NCI Molecular Pathology Unit for assistance with slide imaging. This work was supported by the Intramural Research Program of the National Cancer Institute, NIH (to PSM and PDA, grant numbers ZIA SC0130378, SC010379, BC010982), the William C. and Joyce C. O'Neil Charitable Trust, Memorial Sloan Kettering Single Cell Sequencing Initiative (to TB), and NIH R01 CA130995 (to SCP). SWL is an investigator for the Howard Hughes Medical Institute and the Geoffrey Beene Chair of Cancer Biology.

Address correspondence to: Peter D. Aplan, Genetics Branch, Center for Cancer Research, National Cancer Institute, NIH, Building 37, Room 6002, 37 Convent Drive, Bethesda, Maryland 20892, USA. Phone: 240.760.6889; Email: aplanp@mail.nih.gov.

1. Gaillard H, García-Muse T, Aguilera A. Replication stress and cancer. *Nat Rev Cancer*. 2015;15(5):276–289.
2. Hills SA, Diffley JF. DNA replication and oncogene-induced replicative stress. *Curr Biol*. 2014;24(10):R435–R444.
3. Tubbs A, Nussenzweig A. Endogenous DNA damage as a source of genomic instability in cancer. *Cell*. 2017;168(4):644–656.
4. Evrin C, et al. A double-hexameric MCM2-7 complex is loaded onto origin DNA during licensing of eukaryotic DNA replication. *Proc Natl Acad Sci USA*. 2009;106(48):20240–20245.
5. Ticau S, Friedman LJ, Champasa K, Corrêa IR, Gelles J, Bell SP. Mechanism and timing of Mcm2-7 ring closure during DNA replication origin licensing. *Nat Struct Mol Biol*. 2017;24(3):309–315.
6. Pruitt SC, Bailey KJ, Freeland A. Reduced Mcm2 expression results in severe stem/progenitor cell deficiency and cancer. *Stem Cells*. 2007;25(12):3121–3132.
7. Ibarra A, Schwob E, Méndez J. Excess MCM proteins protect human cells from replicative stress by licensing backup origins of replication. *Proc Natl Acad Sci USA*. 2008;105(26):8956–8961.
8. Orr SJ, et al. Reducing MCM levels in human primary T cells during the G(0)-->G(1) transition causes genomic instability during the first cell cycle. *Oncogene*. 2010;29(26):3803–3814.
9. Rusiniak ME, Kunnev D, Freeland A, Cady GK, Pruitt SC. Mcm2 deficiency results in short deletions allowing high resolution identification of genes contributing to lymphoblastic lymphoma. *Oncogene*. 2012;31(36):4034–4044.
10. Muller HJ. Artificial transmutation of the gene. *Science*. 1927;66(1699):84–87.
11. Brown SD, Nolan PM. Mouse mutagenesis-systematic studies of mammalian gene function. *Hum Mol Genet*. 1998;7(10):1627–1633.
12. Li J, et al. Leukaemia disease genes: large-scale cloning and pathway predictions. *Nat Genet*. 1999;23(3):348–353.

13. Raza-Egilmez SZ, Jani-Sait SN, Grossi M, Higgins MJ, Shows TB, Aplan PD. NUP98-HOXD13 gene fusion in therapy-related acute myelogenous leukemia. *Cancer Res*. 1998;58(19):4269–4273.
14. Lin YW, Slape C, Zhang Z, Aplan PD. NUP98-HOXD13 transgenic mice develop a highly penetrant, severe myelodysplastic syndrome that progresses to acute leukemia. *Blood*. 2005;106(1):287–295.
15. Slape C, Liu LY, Beachy S, Aplan PD. Leukemic transformation in mice expressing a NUP98-HOXD13 transgene is accompanied by spontaneous mutations in Nras, Kras, and Cbl. *Blood*. 2008;112(5):2017–2019.
16. Slape C, Hartung H, Lin YW, Bies J, Wolff L, Aplan PD. Retroviral insertional mutagenesis identifies genes that collaborate with NUP98-HOXD13 during leukemic transformation. *Cancer Res*. 2007;67(11):5148–5155.
17. Suzuki T, et al. New genes involved in cancer identified by retroviral tagging. *Nat Genet*. 2002;32(1):166–174.
18. Gough SM, Chung YJ, Aplan PD. Depletion of cytotoxic T-cells does not protect NUP98-HOXD13 mice from myelodysplastic syndrome but reveals a modest tumor immunosurveillance effect. *PLoS ONE*. 2012;7(5):e36876.
19. Baslan T, et al. Optimizing sparse sequencing of single cells for highly multiplex copy number profiling. *Genome Res*. 2015;25(5):714–724.
20. Tesio M, et al. Age-related clinical and biological features of PTEN abnormalities in T-cell acute lymphoblastic leukaemia. *Leukemia*. 2017;31(12):2594–2600.
21. Bain G, et al. E2A deficiency leads to abnormalities in alphabeta T-cell development and to rapid development of T-cell lymphomas. *Mol Cell Biol*. 1997;17(8):4782–4791.
22. Watanabe M, et al. Downregulation of CDKN1A in adult T-cell leukemia/lymphoma despite overexpression of CDKN1A in human T-lymphotropic virus 1-infected cell lines. *J Virol*. 2010;84(14):6966–6977.
23. Gutierrez A, et al. The BCL11B tumor suppressor is mutated across the major molecular subtypes of T-cell acute lymphoblastic leukemia. *Blood*. 2011;118(15):4169–4173.
24. Liu Y, et al. The genomic landscape of pediatric and young adult T-lineage acute lymphoblastic leukemia. *Nat Genet*. 2017;49(8):1211–1218.
25. Olsson L, Johansson B. Ikaros and leukaemia. *Br J Haematol*. 2015;169(4):479–491.
26. Weng AP, et al. Activating mutations of NOTCH1 in human T cell acute lymphoblastic leukemia. *Science*. 2004;306(5694):269–271.
27. Lin YW, Nichols RA, Letterio JJ, Aplan PD. Notch1 mutations are important for leukemic transformation in murine models of precursor-T leukemia/lymphoma. *Blood*. 2006;107(6):2540–2543.
28. Ashworth TD, et al. Deletion-based mechanisms of Notch1 activation in T-ALL: key roles for RAG recombinase and a conserved internal translational start site in Notch1. *Blood*. 2010;116(25):5455–5464.
29. Gough SM, et al. NUP98-PHF23 is a chromatin-modifying oncoprotein that causes a wide array of leukemias sensitive to inhibition of PHD histone reader function. *Cancer Discov*. 2014;4(5):564–577.
30. Killian JK, et al. Recurrent epimutation of SDHC in gastrointestinal stromal tumors. *Sci Transl Med*. 2014;6(268):268ra177.
31. Graux C, et al. Fusion of NUP214 to ABL1 on amplified episomes in T-cell acute lymphoblastic leukemia. *Nat Genet*. 2004;36(10):1084–1089.
32. Eyre T, et al. Episomal amplification of NUP214-ABL1 fusion gene in B-cell acute lymphoblastic leukemia. *Blood*. 2012;120(22):4441–4443.
33. Capdeville R, Buchdunger E, Zimmermann J, Matter A. Glivec (STI571, imatinib), a rationally developed, targeted anticancer drug. *Nat Rev Drug Discov*. 2002;1(7):493–502.
34. Cheng Y, et al. LNK/SH2B3 regulates IL-7 receptor signaling in normal and malignant B-progenitors. *J Clin Invest*. 2016;126(4):1267–1281.
35. Barbosa TC, et al. Impact of mutations in FLT3, PTPN11 and RAS genes on the overall survival of pediatric B cell precursor acute lymphoblastic leukemia in Brazil. *Leuk Lymphoma*. 2014;55(7):1501–1509.
36. Tubbs A, et al. Dual roles of poly(dA:dT) tracts in replication initiation and fork collapse. *Cell*. 2018;174(5):1127–1142.e19.
37. Ma CX, Janetka JW, Piwnica-Worms H. Death by releasing the breaks: CHK1 inhibitors as cancer therapeutics. *Trends Mol Med*. 2011;17(2):88–96.
38. Wallace MD, Southard TL, Schimenti KJ, Schimenti JC. Role of DNA damage response pathways in preventing carcinogenesis caused by intrinsic replication stress. *Oncogene*. 2014;33(28):3688–3695.
39. Alvarez S, et al. Replication stress caused by low MCM expression limits fetal erythropoiesis and hematopoietic stem cell functionality. *Nat Commun*. 2015;6:8548.
40. Kunnev D, Rusiniak ME, Kudla A, Freeland A, Cady GK, Pruitt SC. DNA damage response and tumorigenesis in Mcm2-deficient mice. *Oncogene*. 2010;29(25):3630–3638.
41. Shima N, et al. A viable allele of Mcm4 causes chromosome instability and mammary adenocarcinomas in mice. *Nat Genet*. 2007;39(1):93–98.
42. Gras E, et al. Microsatellite instability, MLH-1 promoter hypermethylation, and frameshift mutations at coding mononucleotide repeat microsatellites in ovarian tumors. *Cancer*. 2001;92(11):2829–2836.
43. Kelkar YD, Strubczewski N, Hile SE, Chiaromonte F, Eckert KA, Makova KD. What is a microsatellite: a computational and experimental definition based upon repeat mutational behavior at A/T and GT/AC repeats. *Genome Biol Evol*. 2010;2:620–635.
44. Hagenbeek TJ, Spits H. T-cell lymphomas in T-cell-specific Pten-deficient mice originate in the thymus. *Leukemia*. 2008;22(3):608–619.
45. Chervinsky DS, Zhao XF, Lam DH, Ellsworth M, Gross KW, Aplan PD. Disordered T-cell development and T-cell malignancies in SCL LMO1 double-transgenic mice: parallels with E2A-deficient mice. *Mol Cell Biol*. 1999;19(7):5025–5035.
46. Chung KY, et al. Enforced expression of NUP98-HOXA9 in human CD34(+) cells enhances stem cell proliferation. *Cancer Res*. 2006;66(24):11781–11791.
47. Mayle A, et al. Dnmt3a loss predisposes murine hematopoietic stem cells to malignant transformation. *Blood*. 2015;125(4):629–638.
48. Goldberg L, et al. Somatic mutations in murine models of leukemia and lymphoma: Disease specificity and clinical relevance. *Genes Chromosomes Cancer*. 2017;56(6):472–483.
49. Gough SM, et al. Progenitor B-1 B-cell acute lymphoblastic leukemia is associated with collaborative mutations in 3 critical pathways. *Blood Adv*. 2017;1(20):1749–1759.

50. Hunger SP, Mullighan CG. Redefining ALL classification: toward detecting high-risk ALL and implementing precision medicine. *Blood*. 2015;125(26):3977–3987.
51. Dubé N, Bourdeau A, Heinonen KM, Cheng A, Loy AL, Tremblay ML. Genetic ablation of protein tyrosine phosphatase 1B accelerates lymphomagenesis of p53-null mice through the regulation of B-cell development. *Cancer Res*. 2005;65(21):10088–10095.
52. Pike KA, Tremblay ML. TC-PTP and PTP1B: Regulating JAK-STAT signaling, controlling lymphoid malignancies. *Cytokine*. 2016;82:52–57.
53. Kleppe M, et al. Deletion of the protein tyrosine phosphatase gene PTPN2 in T-cell acute lymphoblastic leukemia. *Nat Genet*. 2010;42(6):530–535.
54. Morse HC, et al. Bethesda proposals for classification of lymphoid neoplasms in mice. *Blood*. 2002;100(1):246–258.
55. Baslan T, et al. Genome-wide copy number analysis of single cells. *Nat Protoc*. 2012;7(6):1024–1041.
56. DePristo MA, et al. A framework for variation discovery and genotyping using next-generation DNA sequencing data. *Nat Genet*. 2011;43(5):491–498.
57. Van der Auwera GA, et al. From FastQ data to high confidence variant calls: the Genome Analysis Toolkit best practices pipeline. *Curr Protoc Bioinformatics*. 2013;43:11.10.1–11.1033.
58. Li H, Durbin R. Fast and accurate short read alignment with Burrows-Wheeler transform. *Bioinformatics*. 2009;25(14):1754–1760.
59. McKenna A, et al. The Genome Analysis Toolkit: a MapReduce framework for analyzing next-generation DNA sequencing data. *Genome Res*. 2010;20(9):1297–1303.
60. Cibulskis K, et al. Sensitive detection of somatic point mutations in impure and heterogeneous cancer samples. *Nat Biotechnol*. 2013;31(3):213–219.
61. Cingolani P, et al. A program for annotating and predicting the effects of single nucleotide polymorphisms, SnpEff: SNPs in the genome of Drosophila melanogaster strain w1118; iso-2; iso-3. *Fly (Austin)*. 2012;6(2):80–92.
62. Layer RM, Chiang C, Quinlan AR, Hall IM. LUMPY: a probabilistic framework for structural variant discovery. *Genome Biol*. 2014;15(6):R84.
63. Quinlan AR. BEDTools: the Swiss-Army tool for genome feature analysis. *Curr Protoc Bioinformatics*. 2014;47:11.12.1–11.1234.
64. Benson G. Tandem repeats finder: a program to analyze DNA sequences. *Nucleic Acids Res*. 1999;27(2):573–580.